NASA Technical Memorandum 88355

USAAVSCOM Technical Memorandum 86-A-5

Full-Potential Modeling of Blade-Vortex Interactions

H.E. Jones and F.X. Caradonna

August 1986

National Aeronautics and Space Administration

United States Army Aviation Systems Command

NASA Technical Memorandum 88355 USAAVSCOM Technical Memorandum 86-A-5

Full-Potential Modeling of Blade-Vortex Interactions

H. E. Jones,
F. X. Caradonna, Aeroflightdynamics Directorate, U. S. Army Aviation Research and Technology Activity, Ames Research Center, Moffett Field, California

August 1986

National Aeronautics and Space Administration

Ames Research Center
Moffett Field, California 94035

United States Army
Aviation Systems
Command
St. Louis, Missouri 63120

FULL POTENTIAL MODELING OF BLADE-VORTEX INTERACTIONS

H. E. Jones, and F. X. Caradonna

U.S. Army Aeroflightdynamics Directorate, AVSCOM
NASA Ames Research Center
Moffett Field, California 94035 USA

ABSTRACT

A comparison is made of four different models for predicting the unsteady loading induced by a vortex passing close to an airfoil. 1) The first model approximates the vortex effect as a change in the airfoil angle of attack. 2) The second model is related to the first but, instead of imposing only a constant velocity on the airfoil, the distributed effect of the vortex is computed and used. This is analogous to a lifting surface method. 3)The third model is to specify a branch cut discontinuity in the potential field. The vortex is modeled as a jump in potential across the branch cut, the edge of which represents the center of the vortex. 4) The fourth method models the vortex by expressing the potential as the sum of a known potential due to the vortex and an unknown perturbation due to the airfoil. The purpose of the current study is to investigate the four vortex models described above and to determine their relative merits and suitability for use in large three-dimensional codes.

SYMBOLS

$\mathbf{A_1}$	chordwise metric
$\mathbf{A_2}$	cross derivative metric
$\mathbf{A_3}$	chord-normal metric
a	vortex core radius normalized by c
a_∞	freestream speed of sound
$\mathbf{C^*}$	conservation correction terms in algorithm
C_p	pressure coefficient
C_{lV}	vortex strength expressed in equivalent lift coefficient $= 2\tilde{\Gamma}/M_\infty$
c	rotor chord length
G	prescribed vorticity velocity potential
I	identity matrix
i	chordwise grid index
J	Jacobian of coordinate transform matrix (at the node)

j	chord-normal grid index
$\mathbf{L}$	time update operator on left hand side of algorithm
M_∞	freestream Mach number
M_R	relative Mach number of equivalent steady coordinate for blade-vortex interaction (BVI)
N	superscript representing current time level
$\hat{N}$	stream-normal distance in real space, normalized by c
$\mathbf{q}$	velocity vector
$\mathbf{r}$	radial distance from the vortex, normalized by c
$\mathbf{R}$	right side solution vector
$\mathbf{R}^*$	spacial flux terms on right side of algorithm
$\mathbf{S}$	streamwise distance in real space, normalized by c
t	time in chords traveled $= \tilde{t}a_\infty/c$
$\mathbf{U}$	chordwise contravariant velocity vector
u	chordwise velocity, normalized by a_∞
$\mathbf{V}$	chord-normal contravariant velocity vector
v	chord-normal velocity, normalized by a_∞
x	chordwise distance normalized by airfoil chord
x'	equivalent steady coordinate for BVI
X_v, Y_v	location of vortex
y	chord-normal distance normalized by airfoil chord
y'	equivalent steady coordinate for BVI
U_v, V_v	vortex velocity
α	airfoil angle of attack
β	$= \rho^{2-\gamma}$
Δt	time step
η	chord-normal distance in computational space
ϵ	angle between grid and airfoil surface
Φ	total velocity potential
ϕ	perturbation velocity potential
Γ	jump in potential across a branch-cut
$\tilde{\Gamma}$	vortex strength
γ	specific heat ratio
ρ	fluid density normalized by freestream values
$\hat{\rho}$	$= \rho/J$
τ	time in computational space (chords traveled)

θ angle between blade and vortex

ξ chordwise distance in computational space

1. INTRODUCTION

Helicopter rotors operating in high-speed flight encounter a number of important aerodynamic phenomena. One of the key features of the aerodynamic environment is the presence of transonic flow conditions. Transonic flow imposes major limitations on the high speed performance of the rotor. These limitations manifest themselves in high vibration levels, power divergence, noise, and component fatigue. Traditional integral methods of computing rotor aerodynamics [1], are unable to assess the full impact of these transonic effects. This is because they rely on linear aerodynamic theories and tabulated airfoil data to compute rotor loads.

Various investigators [2-3] have addressed these limitations by using finite-difference methods to compute rotor aerodynamics. These methods provide the capability to compute the whole transonic nonlinear flow field about the rotor. An essential difference between these nonlinear methods and the linear integral methods is that the linear solutions depend only on the blade surface and shear layer conditions. In contrast, the nonlinear solutions depend on what occurs in the entire flow field. (This dependence on the field is best seen in the integral forms of the flow equations – the Ffowcs- Williams Hawkings equation, for instance where all of the nonlinear terms occur in the volume rather than surface integrals). For rotors, this field dependence is especially noteworthy because the field is frequently occupied with vortices from previous blades. Therefore, an important part of rotor finite-difference computations is the means of specifying vortices. The first finite-difference scheme to include vortices in the flow field [2] was for a potential solution to a high-tip-speed hover problem in which the vortices were specified as edges of potential discontinuities. This scheme produced good comparisons with pressure data. Interestingly, Ref. [2] also reported an inability to obtain good solutions when the effect of the vortex was included only by a blade-surface-inflow specification. The extension of such a vortex scheme to forward flight has not yet occurred because of the much greater geometric complexity of the vortices. To date, the forward flight computations have relied on vortex-induced surface-inflow boundary conditions and have been fairly successful at high advance ratios where the induced flow is a small percentage of the total inflow. Nevertheless, there remains a serious question of how best to introduce moving vortices in a grid and thereby predict their effects.

A rotor interacts with a vortex under a wide range of relative orientations. However, the essential physics can be illustrated by considering a rectangular blade of infinite aspect ratio interacting with an infinite line vortex at an angle θ. Johnson [1] has shown that this problem is steady in a coordinate system with its origin traveling with the intersection of the blade centerline and the projection of the free vortex on the blade (see Fig. 1a). The steady coordinate system is

$$
\begin{aligned}
x' &= x \\
y' &= y - M_\infty \tan\theta
\end{aligned}
\tag{1}
$$

The speed at which the origin travels is a function of the angle θ. When $\theta = \pi/2$, the vortex is perpendicular to the blade and the speed of the interaction point is zero (see Fig. 1b). For increasing values of θ, the speed of the interaction point increases but the problem remains steady. For $\theta = \pi$, there is no spanwise flow dependence and the problem is now 2-D (see Fig. 1c). However, the cost of this 2-D simplification is that this problem is now intrinsically unsteady because the speed of the interaction point is infinite. The blade vortex interaction may then be classified by the two limiting conditions defined by $\theta = \pi/2$ and $\theta = \pi$. The $\theta = \pi/2$ condition may be called a low speed interaction (LSI) since this is a steady problem even in the original coordinate system. The $\theta = \pi$ condition may be called a high speed interaction (HSI) since this is an unsteady problem even in the transformed coordinate system. Both the LSI and the HSI represent real interactions which can have significant affects on the rotor aerodynamics. The LSI, for instance, is the principal type of interaction which occurs during hovering flight. The LSI effects rotor power and low harmonic loading. The HSI occurs during high-speed flight and descents and effects noise, vibrations, and the higher harmonics of loading. Furthermore the HSI contains all of the physics of the LSI therefore the capability to solve for the HSI contains the ability to solve the LSI.

The solution of the HSI problem requires the computation of the time-varying surface pressures during the vortex passage. In the present treatment of the problem, the flow will be assumed to be inviscid and irrotational. This 2-D problem is a convenient testing ground for the vortex modeling schemes that will be required for the full 3-D problem. The 2-D BVI problem will be treated using the unsteady, conservative full-potential finite-difference scheme originally developed by Steger and Caradonna [4]. This scheme will be modified to included various models of the vortex.

2. FORMULATION OF THE FULL-POTENTIAL ALGORITHM

The basic finite-difference code used in this paper is described in Ref. 5. It solves the unsteady, 2-D, full-potential equation in strong conservation form. The mass conservation equation is written in a generalized coordinate system as follows:

$$
\frac{\partial}{\partial\tau}\left(\frac{\rho}{J}\right) + \frac{\partial}{\partial\xi}\left(\frac{\rho \mathbf{U}}{J}\right) + \frac{\partial}{\partial\eta}\left(\frac{\rho \mathbf{V}}{J}\right) = 0 \tag{2}
$$

with density given by

$$
\rho = \left\{1 + \frac{\gamma - 1}{2}\left[M_\infty - 2\Phi_\tau - (\mathbf{U} + \xi_t)\Phi_\xi - (\mathbf{V} + \eta_t)\Phi_\eta\right]\right\}^{\frac{1}{\gamma - 1}} \tag{3}
$$

where $\mathbf{U}$ and $\mathbf{V}$ are the contravariant velocities perpendicular to the η and ξ directions respectively

$$\begin{aligned} U &= \xi_t + \mathbf{A_1}\Phi_\xi + \mathbf{A_2}\Phi_\eta \\ V &= \eta_t + \mathbf{A_2}\Phi_\xi + \mathbf{A_3}\Phi_\eta \end{aligned} \tag{4}$$

and the metric terms $\mathbf{A_1}$,$\mathbf{A_2}$,$\mathbf{A_3}$ are

$$\begin{aligned} \mathbf{A_1} &= \xi_x^2 + \xi_y^2 \\ \mathbf{A_2} &= \xi_x\eta_x + \xi_y\eta_y \\ \mathbf{A_3} &= \eta_x^2 + \eta_y^2 \end{aligned} \tag{5}$$

All velocities are normalized by a_∞: distances by the airfoil chord length and time by the combination (c/a_∞). Density is normalized by the freestream value.

Equation (2) is solved by using first-order backward differencing in time and second-order central differencing in space. The temporal density derivative is locally linearized about the old time levels in a manner that preserves the conservative form (see Ref. 5).

The resulting difference equation is solved by approximately factoring it into ξ and η operators.

$$\begin{aligned} &\left[I + \Delta t U^N \delta_\xi - \frac{\Delta t^2}{\hat{\beta}^N}\delta_\xi(\hat{\rho}A_1)^N\delta_\xi\right] \times \left[I + \Delta t V^N \delta_\eta - \frac{\Delta t^2}{\hat{\beta}^N}\delta_\eta(\hat{\rho}A_2)^N\delta_\eta\right] \times \\ &(\Phi^{N+1} - \Phi^N) = \frac{\Delta t^2}{\hat{\beta}^N}\left[\delta_\xi(\hat{\rho}\bar{U})^N + \delta_\eta(\hat{\rho}\bar{V})^N\right] + C^* \end{aligned} \tag{6}$$

where δ_ξ and δ_η represent central difference operators in space and the term C^* is given by Eq. (7). The bracketed term in Eq. (7) represents the temporal conservation correction to the algorithm.

$$\begin{aligned} C^* = &(\Phi^N - \Phi^{N-1}) + \left[\frac{\hat{\beta}^{N-1}}{\hat{\beta}^N}(\Phi^N - 2\Phi^{N-1} + \Phi^{N-2}) + \frac{\Delta t}{\hat{\beta}^N}(\hat{\rho}^N - \hat{\rho}^{N-1})\right. \\ &\left. + \Delta t\frac{\hat{\beta}^{N-1}}{\hat{\beta}^N}(U^{N-1}\delta_\xi + V^{N-1}\delta_\eta)(\Phi^N - \Phi^{N-1})\right] \end{aligned} \tag{7}$$

Equation 6 may be written in the following compact form

$$\mathbf{L} = \mathbf{R}^* + \mathbf{C} \tag{8}$$

where $\mathbf{L}$ is the update operator and $\mathbf{R}^*$ is the right hand side residual. A steady state ADI relaxation algorithm can be obtained from Eq. (5) by omitting the unsteady C^* term on the right-hand side of the equation. The streamwise flux terms use upwind density biasing in regions of supercritical flow to ensure stability of the algorithm. Details are given in Ref. 5.

3. GRID AND BOUNDARY CONDITIONS

For coding and vortex-modeling simplicity, an orthogonal H mesh is used with the current method. The streamlines and potential lines which surround an airfoil in incompressible flow form such a grid. This type of grid may be computed by means of a complex mapping solution. Since the grid is orthogonal, the metric term $\mathbf{A_2}$ is identically zero. Furthermore, since the grid is steady, the contravariant velocities become

$$\begin{aligned} \mathbf{U} &= \mathbf{A_1}\Phi_\xi \\ \mathbf{V} &= \mathbf{A_3}\Phi_\eta \end{aligned} \tag{9}$$

There are four boundary conditions which are imposed on the flow: (1) the airfoil surface, (2) the outer boundary of the grid, (3) the aft face of the grid, and (4) the Kutta condition.

For inviscid flow, the surface boundary condition requires that the flow be tangential to the airfoil surface. This can be obtained by setting the contravariant velocity $\mathbf{V}$ to zero. For a mesh which exactly conforms to the airfoil this leads to $\Phi_\eta = 0$. One problem with employing this boundary condition is that a new mesh must be generated with every new airfoil or airfoil orientation. An alternative to computing a new grid is to use a transpiration rather than a "no flow" boundary condition. This approach uses a fixed grid which conforms to some convenient profile (e.g., a Joukowski airfoil) which approximates the desired profile. The flow must therefore pass through the grid surface at an angle ϵ which is the difference in angle between the grid surface and the actual surface (see Fig. 2). The flow normal to the grid surface $\Phi_{\hat{N}}$, is

$$\Phi_{\hat{N}} = \Phi_S \tan(\epsilon) \tag{10}$$

where Φ_S is the flow velocity tangent to the grid surface. This condition is merely a generalization of the usual small-disturbance boundary condition (with no leading edge singularity).

Along the outer boundaries, the flow is required to return to undisturbed conditions. Computational outer-boundaries are often so close to the the airfoil surface that this condition cannot produce an accurate or stable result. For these close-grid boundaries, special nonreflective boundary conditions are imposed. However, the current grid boundaries are

sufficiently far away (155 chords horizontally , and 80 chords vertically) so that the assumption of undisturbed flow is valid. The outer boundaries conditions are set with a Dirichlet condition

$$\Phi = M_\infty x \tag{11}$$

Along the aft face of the mesh, the flow is also required to be undisturbed. However, since the present method employs a number of branch cuts (lines of potential discontinuity which model vorticity) the potential cannot be easily specified at this boundary. Instead freestream conditions are imposed by modifying the outgoing flux along the aft face so that $\rho = 1$ is insured. Using the Bernoulli condition, an expression for Φ_ξ is derived,

$$\Phi_\xi = \frac{1}{\xi_x}\left[M_\infty - \frac{\Phi_\tau}{M_\infty}\right] \tag{12}$$

which is used in the flux computation.

For the lifting conditions, some allowance must be made for a jump in potential across a wake-like branch-cut (Kutta condition). This cut extends from the airfoil trailing edge to the aft face of the mesh (hence precluding the use of Dirichlet boundary conditions along the aft face). The cut is aligned with the mean chord line of the airfoil. In an unsteady flow, the jump in potential, Γ, across the cut must be convected downstream. Using the Bernoulli equation and continuity of density across the cut, the following equation governing the convection of vorticity from the trailing edge is derived,

$$\Gamma_\tau + \langle \mathbf{U} \rangle \Gamma_\xi = 0 \tag{13}$$

where $\langle \mathbf{U} \rangle$ is the average of the velocities above and below the branch cut. Equation 13 is used to determine the value of Γ along the branch-cut.

4. VORTEX MODELS

In the previous section, an algorithm for solving for the full-potential flow field around an airfoil in transonic flow was presented. This algorithm will now be modified to include the effect of a 2-D vortex passing near the airfoil. Four models for the vortex will be employed :(1) the angle-of-attack method, (2) the lifting-surface method, (3)the branch-cut method, and (4) the split-potential method. These methods may be grouped into two categories (see Fig. 3).

In the first category are the surface-specification methods. The surface-specification methods model the effect of the vortex on the airfoil surface only, primarily through an imposed inflow velocity on the surface. The angle-of-attack and lifting-surface methods fall into this category. The effect of the vortex on the general flow field is not considered by these models. These models are completely valid for linear flow fields.

For problems characterized by the transonic nonlinearity (that is, with a speed of sound which varies throughout the flow field) a surface effect cannot completely model the effect of the vortex. Therefore it is necessary to explicitly insert the vortex in the flow field. The branch-cut and split-potential models fall into this category.

The classical 2-D vortex model is be used to define the vortex potential

$$\mathbf{G} = \frac{\Gamma}{2\pi}\theta \tag{14}$$

where θ is the angle subtended by the vortex and the field point. The tangential velocity at the field point is

$$V_\theta = \frac{\Gamma}{2\pi \mathbf{r}} \tag{15}$$

The singularity at $r = 0$, is the source of numerical instabilities and requires the use of an artificial core. In the following studies, the model developed by Scully [6] is used. That is

$$V_\theta = \frac{\Gamma}{2\pi \mathbf{r}}\left[\frac{\mathbf{r}^2}{\mathbf{r}^2 + a^2}\right] \tag{16}$$

where a is the vortex core radius.

The vortex is moved through the computational grid by computing the flow velocity at the vortex and integrating over the current time-step to find the update location

$$\begin{aligned} X_v^{N+1} &= X_v^N + U_v \Delta t^N \\ Y_v^{N+1} &= Y_v^N + V_v \Delta t^N \end{aligned} \tag{17}$$

The vortex convection velocities U_v and V_v can be determined by three different methods: (1) a priori specification, (2) interpolation of local flow velocities, and (3) the Biot-Savart law. For the present paper, the vortex is convected at at the free stream speed.

The angle-of-attack method is the simplest possible model of the effect of a vortex on an airfoil. Equation 16 is used to compute the velocity at the airfoil quarter chord. With this velocity a vortex-induced angle of attack is computed (see Fig. 4a). The velocity perpendicular to the chord line is (assuming the leading edge to be at x=0)

$$V_\perp = V_\theta \cos\theta = \frac{\Gamma}{2\pi}\left[\frac{(.25 - X_v)}{\mathbf{r}^2 + a^2}\right] \tag{18}$$

The vortex-induced angle of attack is

$$\alpha_v = \tan^{-1}\frac{V_\perp}{U_\infty} \tag{19}$$

This angle is added to the airfoil angle of attack. The potential field is then computed as before. The angle of attack is updated at each time step as the vortex moves by the airfoil.

The lifting-surface method is the most general form of the surface-specification models. As with the angle-of-attack method, equation 16 is used to compute the induced velocity at the airfoil surface (see Fig. 4b). However, unlike the angle-of-attack method, the velocity is allowed to vary over the surface. This eliminates the major shortcoming of the angle-of-attack method, which is sensitivity to miss distance. For the lifting-surface method, equation 18 is modified

$$V_\perp = V_\theta \cos\theta = \frac{\Gamma}{2\pi}\left[\frac{((x/c) - X_v)}{\mathbf{r}^2 + a^2}\right] \tag{20}$$

With this change, the computation proceeds as before.

Caradonna [7] was the first to use an explicit-method vortex model with a finite-difference rotor computation. The branch-cut method, which he used for steady 3-D flows is based upon the known potential solution for a 2-D vortex, (Eq. 14). This potential is implemented by means of a branch cut which extends from the center of the vortex to the aft face of the computational grid (see Fig. 4c). A jump in potential equal to Γ is imposed across the cut.

At first it would seem that the branch-cut method is well suited to a potential finite-difference algorithm. However, problems arise in unsteady problems whenever the vortex is moved. As the edge of the cut moves past a node, an abrupt change in the local potential occurs. This sharp change gives rise to spurious waves which affect the entire flow field. The problem can be solved by spreading the edge of the branch-cut – which is achieved by distributing vorticity on the various nodes which surround the vortex center. The simplest distribution involves the use of the nearest four grid points. The vortex may be modeled by any arbitrary distribution. Stremel [8], uses a method in which the vortex is modeled with an area weighted distribution of vorticity. The author [5] has used a parabolic distribution of vorticity in the horizontal direction coupled with a vertical linear variation. For the present study the distribution is weighted so that the "center of gravity" of the vorticity represents the center of the vortex. With four grid points, this distribution will uniquely determine the vorticity distribution. Increasing the number of points would require an arbitrary distribution to be imposed upon the vorticity. With this modification, the vortex may be moved from cell to cell smoothly thereby reducing (not eliminating) the spurious waves. The effect of distributing the branch cuts is to create an artificial core for the vortex. The efficacy of the "core" is dependent upon the distribution of the nodes which are in the vicinity of the vortex. Since each of the separate branch cuts represents a separate subvortex and each subvortex has its own singular point, the "core" is very sensitive to the grid geometry.

Another problem associated with moving the vortex is computing the vortex-convection velocity. Interpolation of the local velocities near the vortex is the only available means of computing the vortex velocity directly. The interpolation is complicated by the fact that the vortex creates such a large local disturbance, that it is difficult to separate

the effect of the flow field on the vortex from the effect of the vortex on the flow field. One of the major shortcomings of the branch-cut method is that there is no good way to separate the effects because the branch-cut contains the combined potential of the vortex, the free stream, and the airfoil. The vortex induced velocities dominate the flow near the vortex and make an accurate interpolation very difficult. The velocity at the vortex may be approximated by using the Biot-Savart law in conjunction with the lift on the airfoil. In this approach, equation 16 is essentially used in "reverse" with Γ being the jump in potential at the airfoil trailing edge(and hence a measure of the airfoil lift).

Another feature of the branch-cut method is that it depends upon a difference equation to implement the effect of the vortex. That is, the vortex effect is specified entirely by the potential jump, which is represented by the differencing across the branch-cut. The accuracy of this difference is also dependent upon the local grid geometry. It therefore follows that the accuracy of the vortex model will change as the vortex moves through the mesh. The distribution of the vorticity on the mesh further distorts the model by increasing the mesh dependence. A successful branch-cut model is therefore a compromise between an effective core model and an accurate vortex model.

An alternative to the branch-cut method is the split potential-method (see Fig 4d). In this approach, the velocity is assumed to be a combination of a known velocity and a perturbation velocity (see Ref. 12)

$$\mathbf{q} = \nabla\phi + \mathbf{V_G} \tag{21}$$

where $\mathbf{V_G}$ is the known velocity field and $\nabla\phi$ is a perturbation velocity, which need not be small. The total potential for the blade/vortex problem can be split between the perturbation potential (associated with the airfoil) and the potential, G, which describes the vortex velocity field,

$$\Phi = \phi + \mathbf{G} \tag{22}$$

Any potential algorithm may be modified in this way to include the effects of a known velocity component and a perturbation velocity. Furthermore, the potential G need not represent a vortex, but can represent any flow field which independently satisfies the potential equation. When equation 22 is applied to equation 6, the following equation results:

$$\begin{aligned} \mathbf{L}(\rho^N, \Delta\phi^{N+1}) &= \mathbf{R}^*(\rho^N, \phi^N + \mathbf{G}^N) \\ +\mathbf{C}^*(\rho^N, \rho^{N-1}, \phi^N, \phi^{N-1}, \phi^{N-2}, \beta^{N-1}) & \\ +\mathbf{C}^*(\mathbf{G}^N, \mathbf{G}^{N-1}, \mathbf{G}^{N-2}, \beta^{N-1}) & \\ +\Delta\phi^N + \Delta\mathbf{G}^N - \mathbf{L}(\rho^N, \Delta\mathbf{G}^{N+1}) & \end{aligned} \tag{23}$$

The Bernoulli equation undergoes a similar modification

$$\rho^N = \rho(\phi^N + \mathbf{G}^N) \tag{24}$$

The left side of equation 23 is identical to the original algorithm. The right side contains the additional spatial and temporal gradient terms in $\mathbf{G}$, including the update operator $\mathbf{L}(\mathbf{G})$. Implementation of equation 23 has proven to be a challenge to several researchers,[3,9,10] who have sought to simplify the equation. The principal focus of these efforts has been to eliminate the temporal gradient terms in $\mathbf{G}$. These terms pose a particular problem since they involve the potential $\mathbf{G}$ explicitly. Computing this term requires the tracking of a branch cut through the flow in effect reducing the split-potential to a branch-cut model. This will be particularly difficult for the complex geometry of the full 3-D problem. Furthermore, it is advantageous to minimize the computational requirements as much as possible. McCroskey [9], has shown (for a small disturbance formulation) that $\mathbf{L}(\mathbf{G})$, and $\Delta\mathbf{G}^N$ can be eliminated since the vortex potential (equation 14) is a solution to

$$\mathbf{L}\Delta\mathbf{G} = 0. \tag{25}$$

Therefore, a "small disturbance version" of 21 would be

$$\mathbf{L}(\rho^N, \Delta\phi^{N+1}) = \mathbf{R}^*(\rho^N, \phi^N + \mathbf{G}^N) + \Delta\phi^N \tag{26}$$

since $\mathbf{C}^*$ terms are not present in a small disturbance form.

Sankar [10] restricted the solution to his algorithm to a so called "weak split-potential" approach in which the temporal and most of the spatial gradient terms in $\mathbf{G}$ are simply dropped (this is essentialy the lifting- surface method).

The present method is neither a small disturbance or "weak split-potential" form. Even so the algorithm can be simplified using an method suggested by Strawn and presented here first. Begin by recasting equation 23

$$\begin{aligned} \mathbf{L}(\rho^N, \Delta\Phi^{N+1}) &= \mathbf{R}^*(\rho^N, \phi^N + \mathbf{G}^N) \\ +\mathbf{C}^*(\rho^N, \rho^{N-1}, \phi^N, \phi^{N-1}, \phi^{N-2}, \beta^{N-1}) & \\ +\mathbf{C}^*(\mathbf{G}^N, \mathbf{G}^{N-1}, \mathbf{G}^{N-2}, \beta^{N-1}) & \\ +\Delta\phi^N + \Delta\mathbf{G}^N & \end{aligned} \tag{27}$$

The update operator, $\mathbf{L}$, has been recombined to include the total potential. The temporal-conservation correction term $\mathbf{C}^*$ in $\mathbf{G}$ has been retained, since there is no way to effectively separate the $\mathbf{G}$ and ϕ parts of the density. The time-derivative terms are obtained using the chain rule:

$$\mathbf{G}_\tau = \mathbf{G}_\xi \xi_\tau + \mathbf{G}_\eta \eta_\tau + \mathbf{G}_t t_\tau \tag{28}$$

This value may be determined most easily in an axes system fixed to the vortex. In this system, the vortex is fixed and the airfoil to which the grid is attached moves past it. In this system

$$\begin{aligned} \mathbf{G}_t &= 0. \\ \eta_\tau &= -V_v \\ \xi_\tau &= -U_v \end{aligned} \tag{29}$$

therefore,

$$\Delta \mathbf{G} = \Delta t^N \mathbf{G}_\tau \tag{30}$$

Use of equation 30 is necessary because if the term $\mathbf{G}$ itself were used, the branch cut associated with it would have to be tracked which would lead to a branch-cut-type method.

5. COMPARISON OF VORTEX MODELS

A straightforward way of comparing the four vortex models is to compare the induced velocity produced on the airfoil by each model. Figure 5 presents a series of such comparisons for a vortex located at the airfoil leading edge and at selected vertical distances.

Since the angle-of-attack, lifting-surface and split-potential models all make use of the same vortex-velocity equation, the results for these models are similar. The difference between the angle-of-attack model and the others is that it imposes a single representative velocity (namely the quarter-chord value) over the entire chord. This model is based on the assumption that the airfoil may be treated as a single point. This model is valid for airfoil/vortex distances greater than about two chords. Between two-chords and one-chord distance, the velocity variation over the chord becomes significant. At less than one chord, the induced velocity variation is large and the angle-of-attack method breaks down entirely. The lifting-surface and split-potential models both require the distribution of vortex induced velocity at the airfoil surface. Thus the lifting-surface model is a degenerate form of the split-potential method with the induced velocity effect restricted to the airfoil surface.

Comparison of the four vortex-modeling methods will be made with the help of experimental data. Recently, Caradonna et al. [11] presented experimental results for a rotor interacting with a vortex. The rotor had two blades with a constant 0012 airfoil section. The blades were untwisted and the rotor had a teetering hub. The rotor aspect ratio was 7. A vortex was generated upstream of the rotor by a fixed, constant-section, NACA 0015 wing (Fig. 6 depicts the experimental setup). When the rotor blade is at an azimuth angle of 180°, a HSI occurs. Pressure at ten locations on the airfoil surface were measured and these data were presented as a function of time (vortex location) and space (airfoil chord).

The data were collected for several rotor tip speeds and vortex locations. Two of these conditions will be used as reference data in comparing the vortex models. The first condition is for a subcritical flow $M_\infty = 0.536$, and a vertical miss distance of Y_v= -0.433. The second case is for a critical flow, $M_\infty = 0.714$, and the same vertical miss distance.

There are two factors which will compromise the correlation. First, the rotor has a low aspect ratio. Since the present method is strictly 2-D, one should expect to see a higher pressure predicted than measured due to aspect ratio effects. The second factor is the rotational velocity of the rotor. The measurements used in the comparison were made at an azimuth location of 180°. However, the effect of the vortex on the blade begins much earlier. Therefore the blade is experiencing a steadily changing freestream flow modified by the vortex. The variable free stream is not modeled by the current method. For the subcritical case, this will not pose a problem since unsteady effects are small at low Mach numbers. However, the critical case is much more sensitive to this effect. The rotor is experiencing a high transonic speed at the 90° azimuth location which decreases as the blade moves forward. As the speed decreases, the shocks on the airfoil surface begin to collapse. The vortex is encountered during this collapsing process. The computation of this flow field requires a three-dimensional model complete with an accurate unsteady-shock model. This is beyond the capability of the current method.

Figure 7a shows a comparison of lift vs vortex location for the four vortex models for the subcritical case. The four methods show little difference in the initial-condition solution. As the vortex approaches, the curves begin to separate, reflecting the effect of the various methods on the flow field solution. When the vortex is between two and three chords upstream, the separation of the curves becomes large. This region can therefore be considered the outer boundary of the close interaction. The curves continue to separate until they reach a maximum difference when the vortex is at the airfoil leading edge. During the interaction phase, the methods display several interesting features. The angle-of-attack method predicts a rapid (almost instantaneous) change in lift as the vortex passes the quarter-chord. This occures because the airfoil undergoes an abrupt change in angle of attack from negative to positive at this point, in effect inverting the curve. An interesting feature of the branch-cut method is that during the interaction phase it predicts a small "spike" in the loading curve. This occurs when the vortex is in the densest part of the grid and is caused by the locally high velocities predicted by this method. This "spike" increases in size as the Mach number increases. For a very strong interaction (M=0.8, $y_v = -0.25$ and $Cl_v = 0.4$), this "spike" leads to an instability in the algorithm which destroys the solution. The split potential and lifting-surface methods are in agreement overall even though they are somewhat different during the closest part of the interaction. Neither of these methods show any unusual features in their predicted loading histories.

Figure 7b presents the variation of lower-surface leading-edge pressure with vortex location for the four methods. Here the difference between the lifting-surface and split-potential methods is more apparent. The "spike" in the branch-cut loading curve is also more apparent than in the integrated data. This figure highlights the change in pressure on the airfoil caused by the sharp change in lift predicted by the angle-of-attack method.

Figure 7c presents comparisons of measured and computed data for each of the methods. These comparisons must be considered qualitatively valid because of the aspect ratio and unsteady rotational flow field of the experiment. The split-potential, lifting-surface, and branch-cut methods all show qualitatively good comparisons but differ in detail. The angle-of-attack method is clearly not accurate for this condition this is due to the sharp change in lift predicted by the model which does not occur in the experiment.

A more interesting comparison is for a flow condition which is just below critical, that is a flow condition which if undisturbed would remain subcritical. The introduction of a vortex in such a flow field would be expected to drive the flow into a supercritical state. A 0012 airfoil at $\alpha = 0°$ and M=0.714 experiences this type of flow.

Figure 8a presents a comparison of lift vs. vortex location for each of the models at this critical flow condition. Inspection of this figure shows qualitatively the same comparison as the subcritical case. The angle-of-attack methods predicts a sharp "lift inversion" as before. The branch-cut method predicts a "spike" in the loading curve of increased size at this higher Mach number. The split-potential and lifting-surface methods both predict smooth curves.

Figure 8b present the pressure time-histories at the airfoil leading edge. The angle-of attack and lifting surface methods both predict pressure histories which are similar to those at the lower Mach number. However, the branch-cut and split-potential curves are markedly different. Both of these methods predict the presence of shock waves although this is obscured in the branch-cut method by the presence of the "spike". The presence of the shock wave in these models is more easily seen in the comparison of the measured and computed data (Fig. 8c). The lifting-surface and angle-of- attack methods not predict shocks.

The comparisons shown in Figs 8b and 8c show that all four models produce qualitatively similar results. The split-potential and lifting-surface methods produce the most accurate integrated-loads curves. The angle-of-attack and branch-cut methods both generate spurious spikes in the loading curve. Comparison of the pressures predicted with the experiment show that the explicit models accurately predict the onset of critical flow conditions. Numerous computational experiments have indicated that the split-potential method is the most robust of these two methods. It also allows for more control of the vortex modeling because it models the vortex as a specified velocity field. Furthermore, the method is not restricted to modeling vortices and can be used to predict the effect of any flow field which is described by a known, irrotational, potential function. Because of this versatility and robustness, the author recommends this method.

One of the key unanswered questions of the split-potential model is the effect of temporal-difference terms in $\mathbf{G}$, $(\mathbf{C}^*, \mathbf{L}, \Delta\mathbf{G})$ on the solution (Eq. 27). These terms can have a serious impact on a 3-D computation because of the geometric complexity of the wake and the difficulty of computing $\mathbf{G}_t$ for each wake element. Figure 9a shows a comparison of the effects of these terms on the integrated lift curve for a subcritical flow condition. It is obvious that there is little difference between the two curves. However, this flow condition is low-speed and the vortex is not very close to the airfoil (a "weak"

interaction). Figure 9b shows a similar comparison for a close supercritical interaction (a "strong" interaction). Here the effect of the terms is much more apparent. In particular, the G_t terms show a marked effect during the interaction phase and the departure phase. Notice, especially the region in which the slope of the curve undergoes a rapid change. This corresponds to the vortex passing through the airfoil shock. The combination of these velocities (shock and vortex) causes high pressures on the airfoil surface which are reflected in the loading curve. In summary, the G_t terms seem to have little effect on the solution except for strong-interaction cases.

6. CONCLUSIONS

A study of the full-potential modeling of a blade-vortex interaction has been conducted. The primary goal of this study has been to investigate the effectiveness of the various methods of modeling the vortex. The problem was studied within the context of a 2-dimensional model problem, which represents one of the limiting types of blade-vortex interactions. The model problem restricts the interaction to that of an infinite wing with an infinite-line vortex moving parallel to its leading edge. This problem provides a convenient testing ground for the various methods of modeling the vortex while retaining the essential physics of the full 3-D interaction. The flow field can be assumed to be inviscid, irrotational, unsteady, and, in general, transonic. Four different models of the vortex were used. These four models have been compared to each other and to experimental data to determine their relative merits. The following comparisons were made : (a) generated velocity fields, (b) a subcritical interaction, and (c) a critical interaction. The subcritical and critical interactions are also compared with experimentally generated results.

As a result of these comparisons the following conclusions have been reached:

(a) Only the explicit models predict the presence of shock waves for the critical interaction.

(b) The branch-cut method shows a strong sensitivity to the mesh configuration which leads to spurious waves in the solution, especially for transonic flow cases.

(c) The lifting-surface method compares well with the split-potential method, especially for subcritical flow. This method has proven to be useful in 3-D problems to specify far-field vortex effects.

(d) The split-potential method is the most versatile and robust method. The temporal gradient terms in the split-potential method must be retained to predict "strong" interactions. This may cause a slight increase in computing time for 3-D problems, which can be offset by using the lifting surface method for vortices far from the blade.

The primary goal of this study has been to examine the effect of the vortex model on the computation of the BVI problem. The split-potential model has proven to be the most versatile and robust method of the currently available techniques. The lifting-surface method has been shown to be a useful approximation to the split-potential method

especially for far-field vortex specifications. The next logical step in this study is to extend these results to the 3-D rotor problem. In the process of accomplishing this, the method should be coupled with an existing, comprehensive helicopter method, similar to that used by Strawn and Tung [13]. The 3-D model should include a complete vortex wake model using the split-potential method. Another interesting application of the split- potential technique would be to make use of it to model linear portions of the flow field (e. g. the rotational flow field).

The modeling of the BVI will continue to be a key problem in helicopter aerodynamics because it is a major determinant of vibratory loading and noise. This study has analyzed the interaction in two dimensions and used this model problem to find the best means of determining BVI loading within the context of a finite difference computation. The extension to three dimensions should build directly on this work. Beyond this point, the greatest problem will be to find an efficient and accurate way to predict the three dimensional structure of the rotor wake.

8. ACKNOWLEDGMENTS

The authors would like to thank Dr. Roger Strawn of the Army Aeroflightdynamics Directorate, for many hours useful discussion.

7. REFERENCES

1. Johnson W.,"A Lifting Surface Solution for Vortex Airloads and its Application to Rotary Wing Airloads Calculations," ASRL TR-153-2, Apr. 1970.

2. Caradonna, F. X., Desopper, A. and Tung, C., "Finite Difference Modeling of Rotor Flows Including Wake Effects" Paper No. 2.7, *Eighth European Rotorcraft Forum*, Aix-en-Provence, France, Aug. 1982.

3. Strawn, R. C., and Caradonna, F. X.," Numerical Modeling of Rotor Flows with a Conservative Form of the Full-Potential Equations" AIAA Paper 86-0079, Jan. 1986.

4. Steger, J. L., and Caradonna, F. X., "A Conservative Implicit Finite Difference Algorithm for the Unsteady Transonic Full Potential Equation," AIAA Paper 80-1368, Snowmass, Colorado 1980.

5. Jones, H., "Full-Potential Modeling of Blade-Vortex Interactions" Ph. D. thesis, George Washington University, Aug, 1986.

6. Scully, M. P., "Computations of Helicopter Rotor Wake Geometry and Its Influence on Rotor Harmonic Load" ASRL TR-178-1, Massachusetts Institute of Technology, Mar. 1975.

7. Caradonna, F. X., "The Transonic Flow on a Helicopter Rotor" Ph.D. Dissertation, Stanford University, Mar. 1978.

8. Stremel, P. M., "Computational Methods for Non-Planar Vortex Wake Flow Fields with Applications to Conventional and Rotating Wings" Master of Science Thesis, Massachusetts Institute Of Technology, Feb. 1982.

9. McCroskey, W. J. and Goorjian, P. M., "Interactions of Airfoils with Gusts and Concentrated Vortices in Unsteady Transonic Flow" AIAA Paper 83-1691, Danvers, Mass. 1983.

10. Sankar, L. N., and Malone, J. B., "Unsteady Transonic Full Potential Solutions for Airfoils Encountering Vortices and Gusts" AIAA Paper 85-1710, Cincinnati, Ohio 1985.

11. Caradonna, F. X., Laub, G. H., and Tung, C.,"An Experimental Investigation of the Parallel Blade-Vortex Interaction" *Presented at the 10th European Rotorcraft Forum*, Aug. 28-31, 1984, The Hague, Netherlands.

12. Steinhoff, J., "The Treatment of Convected Vorticies in Compressible Potential Flow" Paper No. 22, *Symposium on Aerodynamics of Vortical-Type Flows in Three Dimensions*, AGARD CP-342, 1983.

13. Strawn, R. C. and Tung, C.,"The Prediction of Transonic Loading on Advancing Helicopter Rotors" *Presented at the AGARD/FDP Symposium on Applications of Computational Fluid Dynamics in Aeronautics*, Apr. 7-10, 1986, Aix-en-Provence, France, (see also NASA TM- 88238, April 1986).

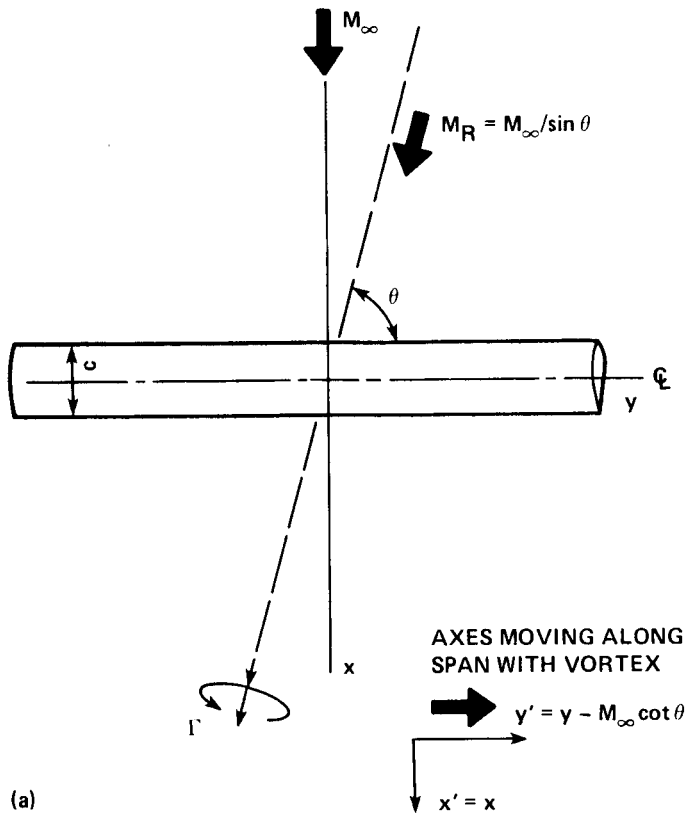

Fig. 1a. The interaction of an infinite aspect ratio blade with an infinite line vortex.

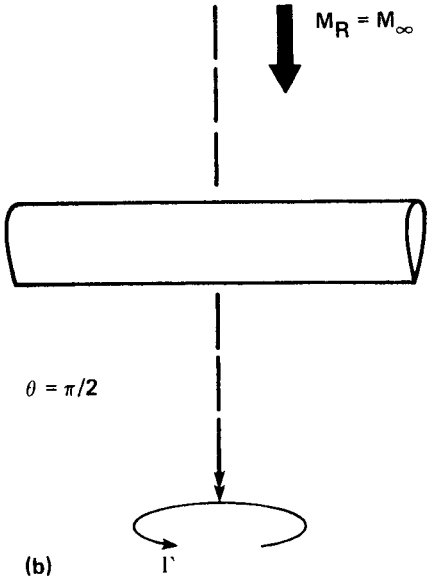

Fig. 1b. The low speed interaction (LSI) between a rotor and a vortex.

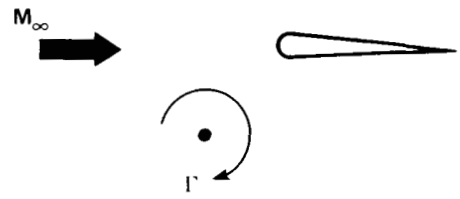

$\theta = \pi$, $M_R = \infty$

(c)

Fig. 1c. The high speed interaction (HSI) between a rotor and a vortex.

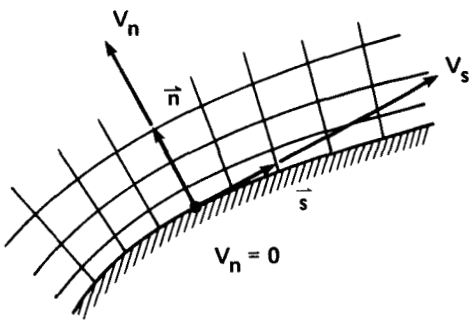

FLOW TANGENCY ON A BODY CONFORMING COORDINATE

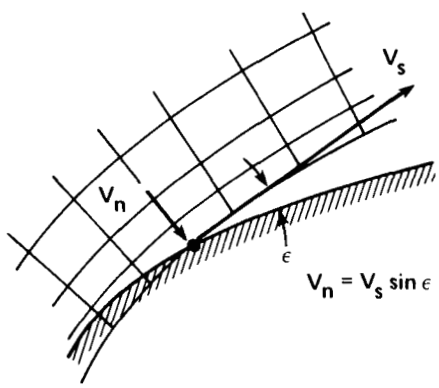

FLOW-THROUGH CONDITION ON A COORDINATE WHICH APPROXIMATES THE BODY (A GENERALIZATION OF THE SMALL DISTURBANCE BOUNDARY CONDITION)

Fig. 2. The transpiration boundary condition at the airfoil surface.

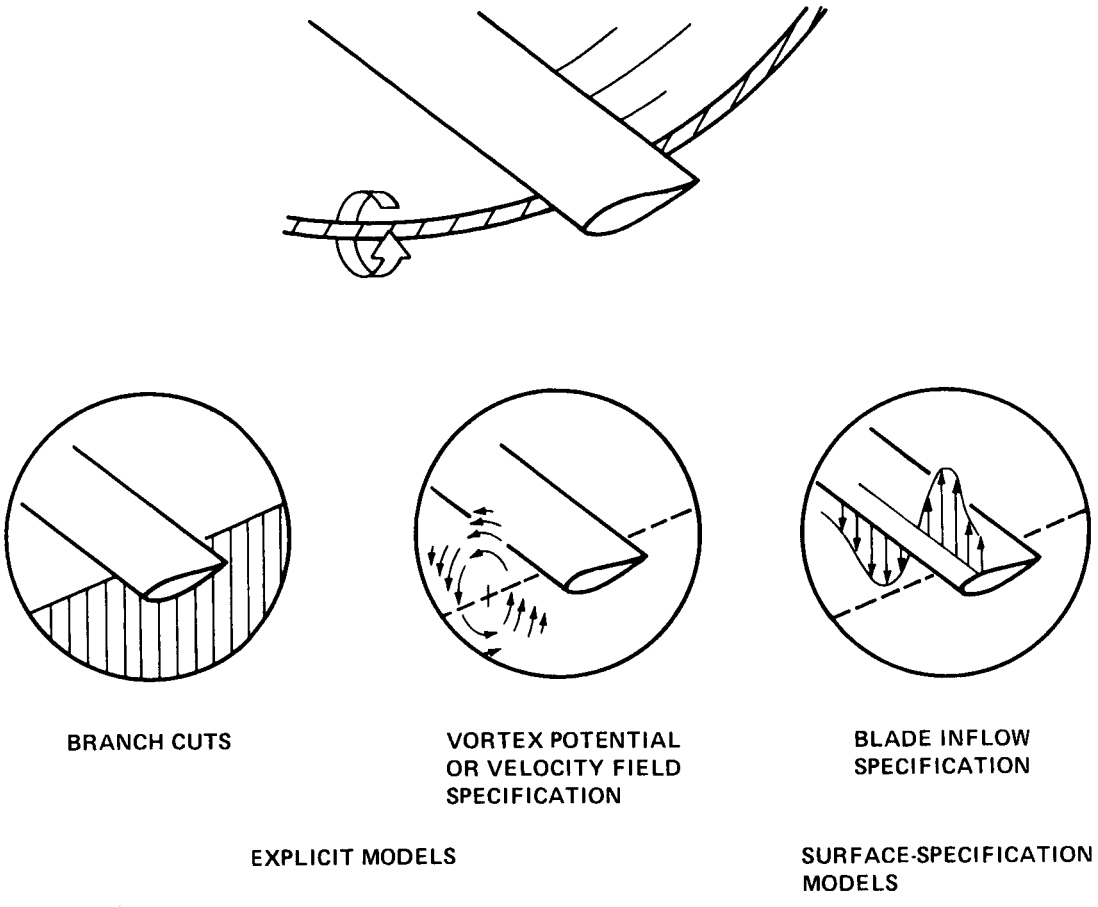

Fig. 3. Principal vortex models.

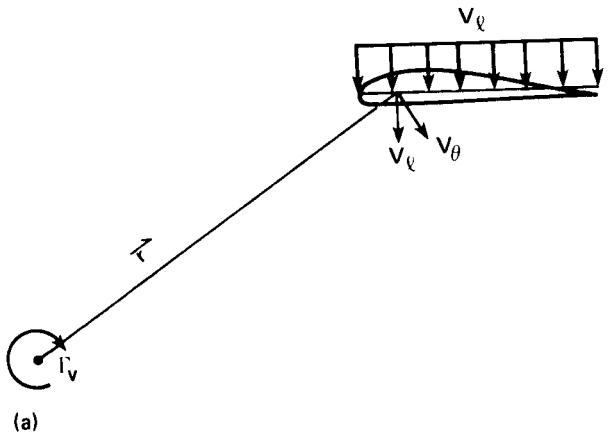

Fig. 4a. Angle-of-attack vortex model.

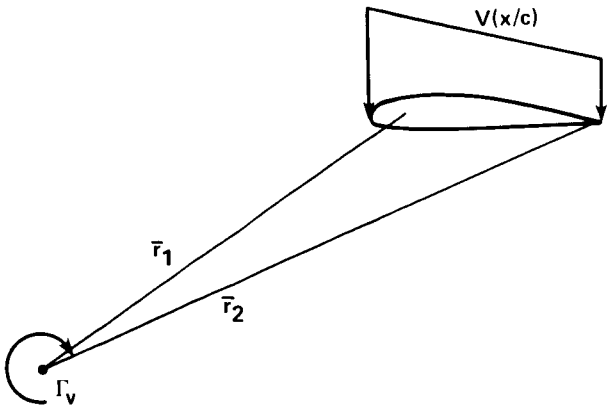

Fig. 4b. Lifting-surface vortex model.

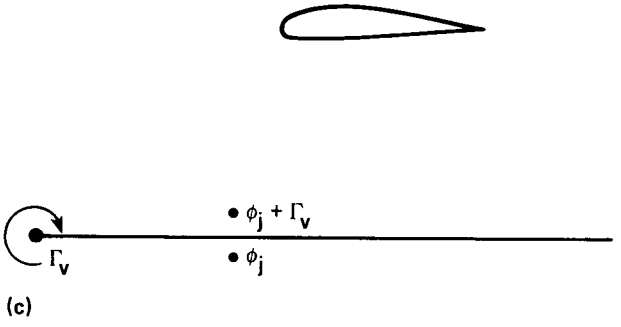

Fig. 4c. Branch-cut vortex model.

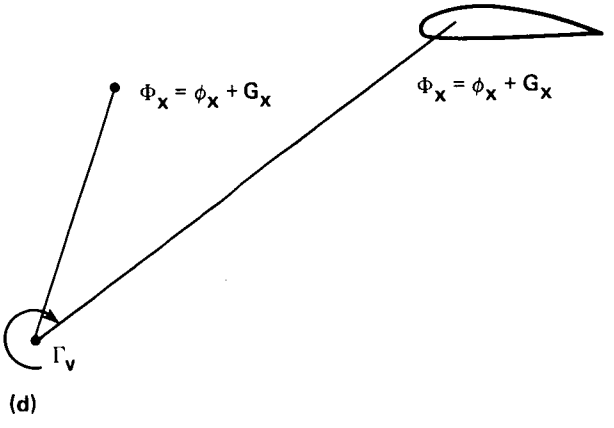

Fig. 4d. Split-potential vortex model.

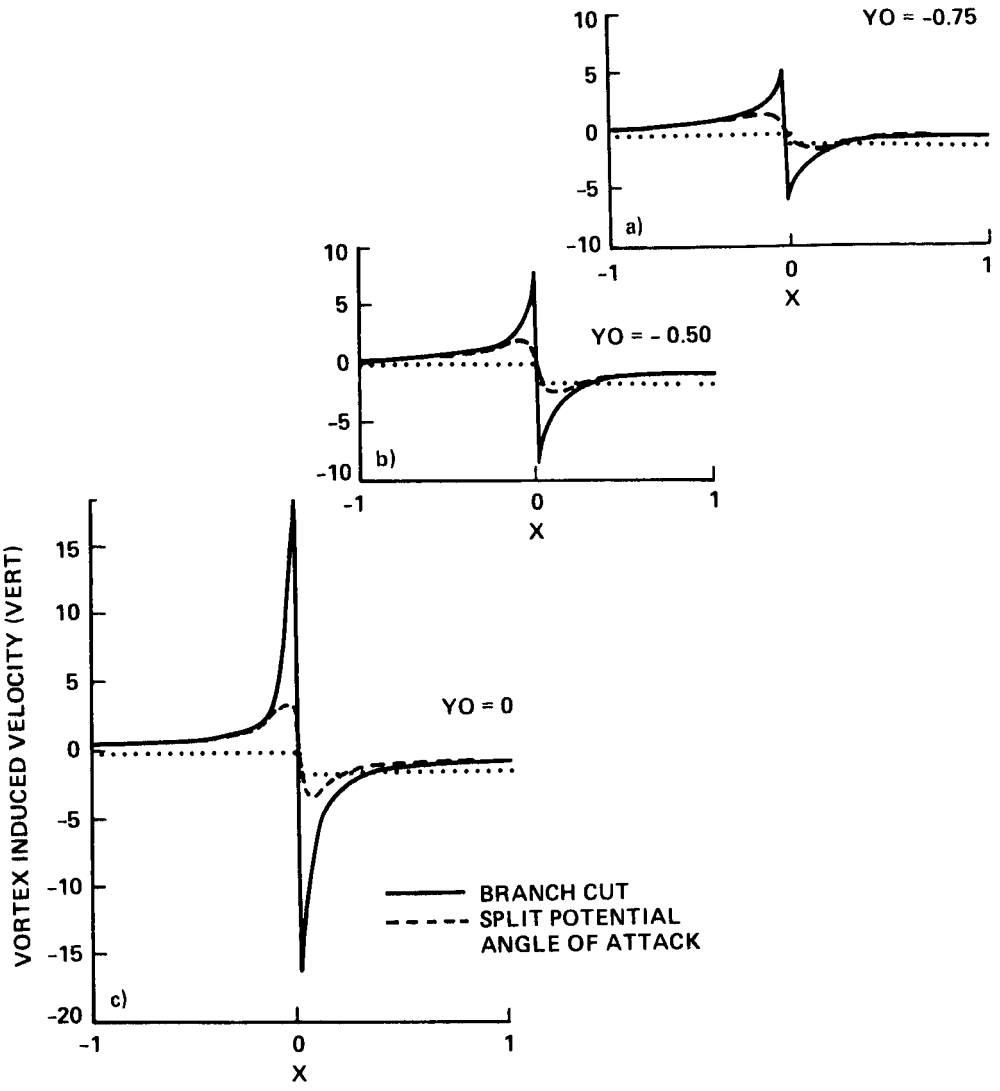

Fig. 5. Vortex induced velocity on airfoil surface.

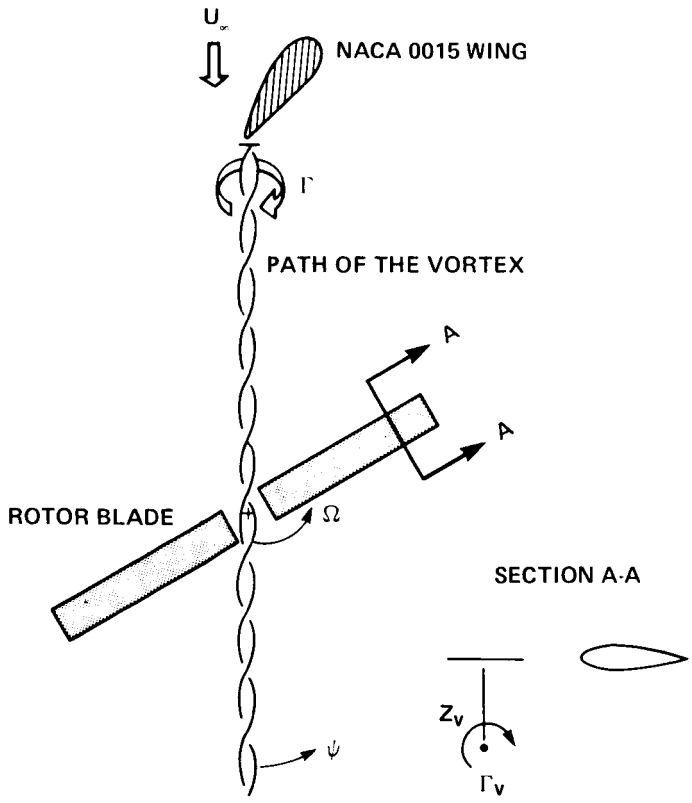

Fig. 6. Experimental measurment of blade-vortex interaction.

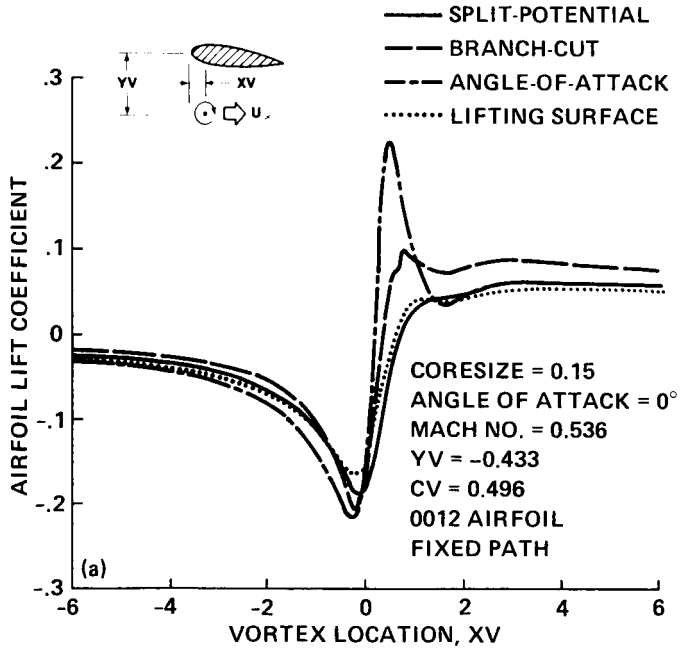

Fig. 7a. Comparison of airfoil lift variation with vortex location for a variety of vortex models, subcritical.

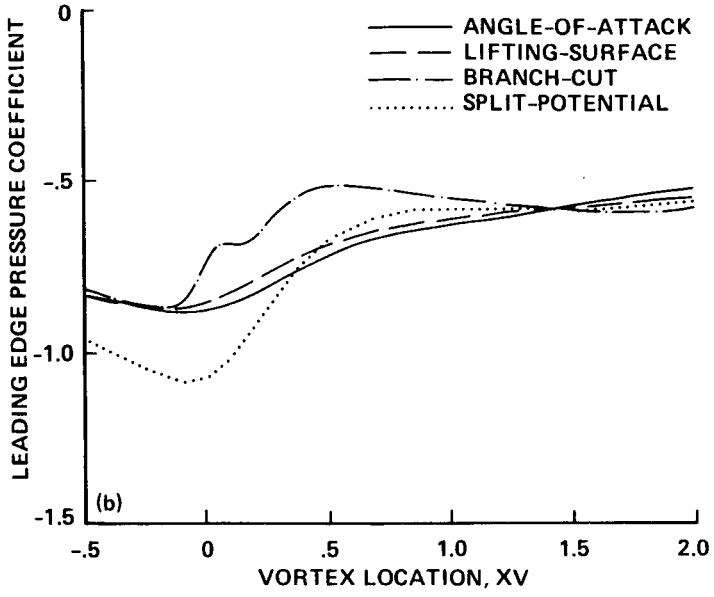

Fig. 7b. Variation of airfoil pressure with vortex location for a variety of vortex models, subcritical.

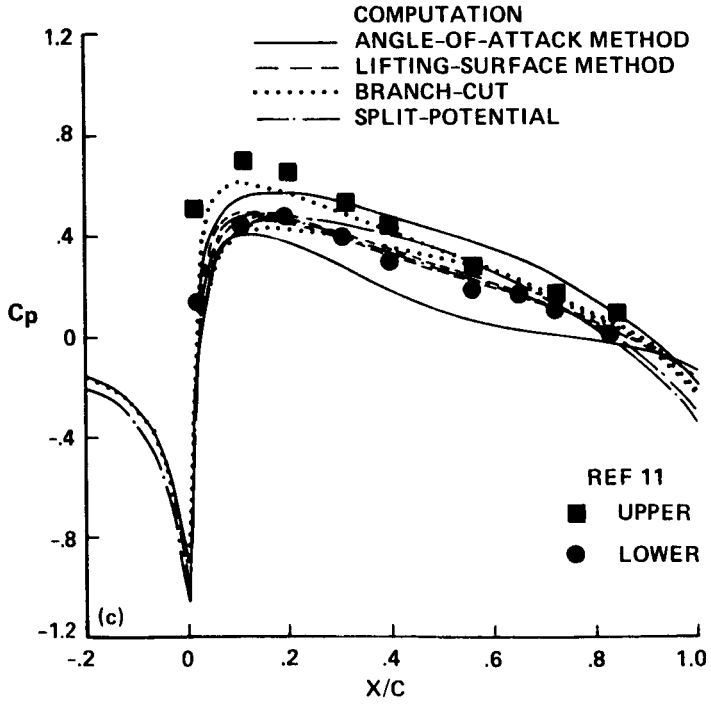

Fig. 7c. Comparison of predicted and measured airfoil surface pressures, for each vortex model $M_\infty = 0.536$, $\alpha = 0$, Y0 = -0.433, X0=0., $C_{l_v} = 0.496$, NACA 0012.

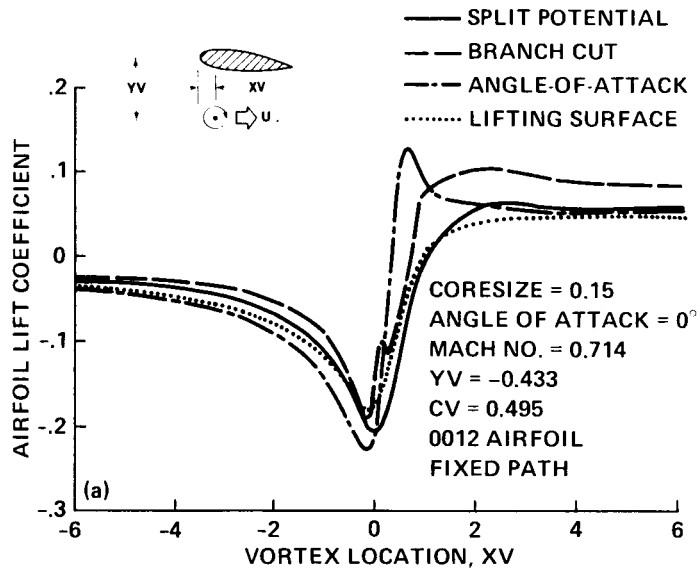

Fig. 8a. Comparison of airfoil lift variation with vortex location for a variety of vortex models, critical.

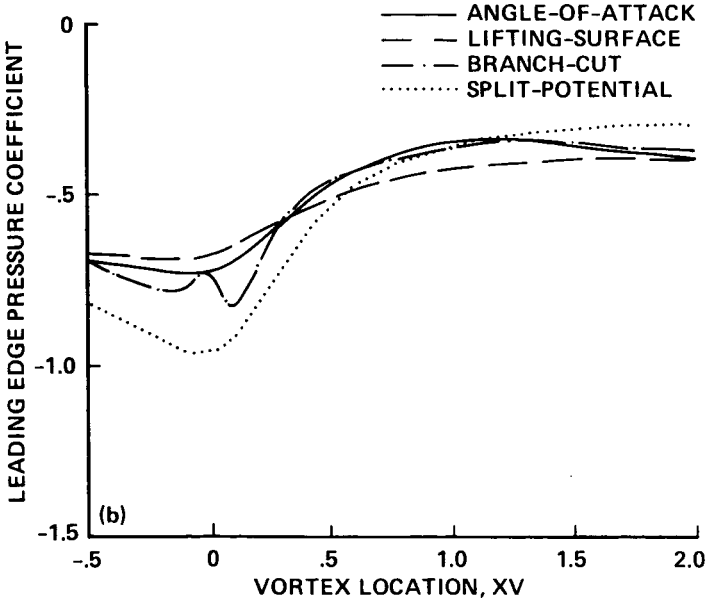

Fig. 8b. Variation of airfoil pressure with vortex location for a variety of vortex models, critical.

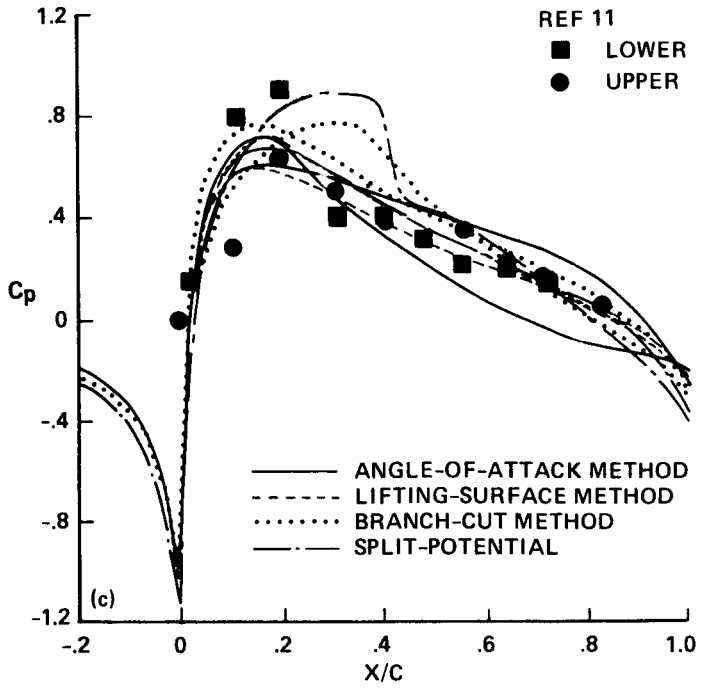

Fig. 8c. Comparison of predicted and measured airfoil surface pressures, for each vortex model $M_\infty = 0.714$, $\alpha = 0$, Y0 = -0.433, X0=0., $C_{l_v} = 0.496$, NACA 0012.

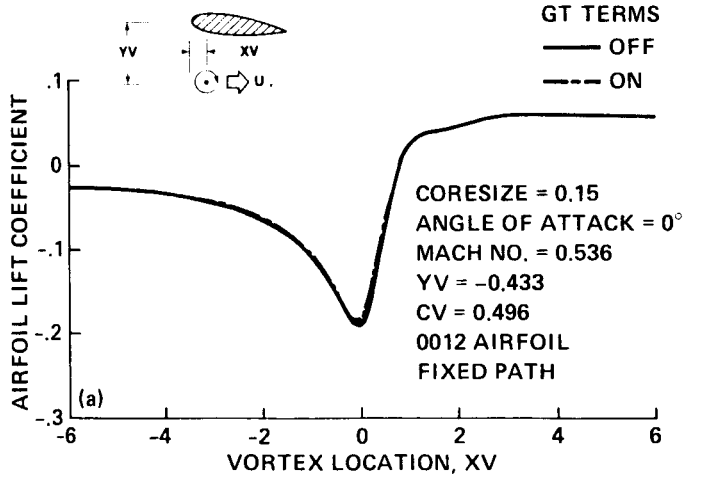

Fig. 9a. Effect of G_t terms on split potential model, subcritical.

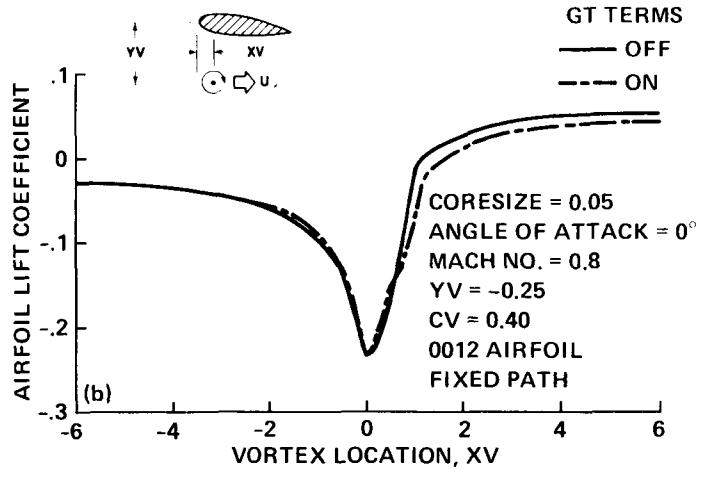

Fig. 9b. Effect of G_t terms on split potential model, supercritical.

1. Report No. NASA TM-88355 and USAAVSCOM TM-86 A-5	2. Government Accession No.	3. Recipient's Catalog No.
4. Title and Subtitle FULL-POTENTIAL MODELING OF BLADE-VORTEX INTERACTIONS		5. Report Date August 1986 6. Performing Organization Code
7. Author(s) H. E. Jones and F. X. Caradonna		8. Performing Organization Report No. A-86395 10. Work Unit No.
9. Performing Organization Name and Address Aeroflightdynamics Directorate, U.S. Army Aviation Research and Technology Activity, Ames Research Center, Moffett Field, CA 94035-1099		11. Contract or Grant No.
12. Sponsoring Agency Name and Address National Aeronautics and Space Administration, Washington, DC 20546 and U.S. Army Aviation Research and Development Command St. Louis, MO 63120		13. Type of Report and Period Covered Technical Memorandum 14. Sponsoring Agency Code 992-21-01

15. Supplementary Notes

Point of Contact: H. E. Jones, Ames Research Center, MS 215-1, Moffett Field, CA 94035 (415) 694-5902 or FTS 464-5902

16. Abstract

A comparison is made of four different models for predicting the unsteady loading induced by a vortex passing close to an airfoil. 1) The first model approximates the vortex effect as a change in the airfoil angle of attack. 2) The second model is related to the first but, instead of imposing only a constant velocity on the airfoil, the distributed effect of the vortex is computed and used. This is analogous to a lifting surface method. 3) The third model is to specify a branch cut discontinuity in the potential field. The vortex is modeled as a jump in potential across the branch cut, the edge of which represents the center of the vortex. 4) The fourth method models the vortex by expressing the potential as the sum of a known potential due to the vortex and an unknown perturbation due to the airfoil. The purpose of the current study is to investigate the four vortex models described above and to determine their relative merits and suitability for use in large three-dimensional codes.

17. Key Words (Suggested by Author(s))	18. Distribution Statement		
Helicopter Vortex interactions Wakes Full potential	Unlimited Subject category - 01		
19. Security Classif. (of this report) Unclassified	20. Security Classif. (of this page) Unclassified	21. No. of Pages 29	22. Price* A03

*For sale by the National Technical Information Service, Springfield, Virginia 22161